AD-A064 865 NAVAL POSTGRADUATE SCHOOL MONTEREY CALIF F/G 17/5
ADVANCED INFRARED DETECTORS FOR FUTURE MISSILE SEEKERS.(U)
DEC 78 R A FANTAUZZO

UNCLASSIFIED NL

| OF |
AD
A064865

END
DATE
FILMED
4-79
DDC

LEVEL II

AD A064865

DDC FILE COPY

NAVAL POSTGRADUATE SCHOOL

Monterey, California

DDC
RECEIVED
FEB 26 1979
A

THESIS

ADVANCED INFRARED DETECTORS FOR FUTURE MISSILE SEEKERS

by

Richard Alan Fantauzzo

December 1978

Thesis Co-Advisors: A. E. Fuhs R. B. Schoolar

Approved for public release; distribution unlimited.

79 02 23 122

UNCLASSIFIED

SECURITY CLASSIFICATION OF THIS PAGE (When Data Entered)

REPORT DOCUMENTATION PAGE		READ INSTRUCTIONS BEFORE COMPLETING FORM
1. REPORT NUMBER	2. GOVT ACCESSION NO.	3. RECIPIENT'S CATALOG NUMBER
4. TITLE (and Subtitle) (6) Advanced Infrared Detectors for Future Missile Seekers.		5. TYPE OF REPORT & PERIOD COVERED (9) Master's Thesis, December 1978
		6. PERFORMING ORG. REPORT NUMBER
7. AUTHOR(s) (10) Richard Alan Fantauzzo		8. CONTRACT OR GRANT NUMBER(s) AFWL Work Order #57294 Segment Number 1133/4
9. PERFORMING ORGANIZATION NAME AND ADDRESS Naval Postgraduate School Monterey, California 93940		10. PROGRAM ELEMENT, PROJECT, TASK AREA & WORK UNIT NUMBERS (12) 66p.
11. CONTROLLING OFFICE NAME AND ADDRESS Naval Postgraduate School Monterey, California 93940		12. REPORT DATE (11) December 1978
		13. NUMBER OF PAGES 65
14. MONITORING AGENCY NAME & ADDRESS (if different from Controlling Office) Naval Postgraduate School Monterey, California 93940		15. SECURITY CLASS. (of this report) Unclassified
		15a. DECLASSIFICATION/DOWNGRADING SCHEDULE

16. DISTRIBUTION STATEMENT (of this Report)

Approved for public release; distribution unlimited.

17. DISTRIBUTION STATEMENT (of the abstract entered in Block 20, if different from Report)

18. SUPPLEMENTARY NOTES

19. KEY WORDS (Continue on reverse side if necessary and identify by block number)

p-n Junction Devices; Metal Semiconductor Devices; Infrared Detectors; Epitaxial Films; Transport Properties; Alloy Semiconductors

PbS(x)Se(1-x).

20. ABSTRACT (Continue on reverse side if necessary and identify by block number)

New technology was utilized to design and fabricate a self-filtering infrared detector (SFD) optimized for a specific target signature. The SFD was prepared from vacuum deposited, composition-tuned epitaxial films of the semiconductor alloy, PbS_xSe_{1-x}. A filter and detector layer were both grown on opposite sides of a BaF_2 substrate. The detector element was a p-n junction formed by depositing a Pb

DD FORM 1 JAN 73 1473 EDITION OF 1 NOV 65 IS OBSOLETE S/N 0102-014-6601

UNCLASSIFIED

SECURITY CLASSIFICATION OF THIS PAGE (When Data Entered)

251 450

contact onto a p-type detector layer surrounded by a Au ohmic contact. The optical cuton and cutoff wavelengths were composition-tuned to 4.0 and 5.0 μm by adjusting x in both layers. The measured spectral response of the SFD device was in good agreement with theoretical calculations, whereas, the quantum efficiency was below. The device resistance was two orders of magnitude below the predicted values due to surface leakage. This leakage also caused the peak responsivity and detectivity to be lower than the predicted values. Application of this technology shows great promise provided these problems can be resolved.

ACCESSION for
NTIS White Section
DDC Buff Section
UNANNOUNCED
JUSTIFICATION
BY
DISTRIBUTION/AVAILABILITY CODES
Dist. AVAIL. and/or SPECIAL
A

79 02 23 122

Approved for public release; distribution unlimited.

Advanced Infrared Detectors for Future Missile Seekers

by

Richard Alan Fantauzzo
Lieutenant Commander, United States Navy
B. S., United States Naval Academy, 1967

Submitted in partial fulfillment of the
requirements for the degree of

MASTER OF SCIENCE IN APPLIED SCIENCE

from the

NAVAL POSTGRADUATE SCHOOL
December 1978

Author Richard A. Fantauzzo

Approved by [signature]
Thesis Co-Advisor

Allen E. Fuhs
Thesis Co-Advisor

[signature]
Chairman, Department of Mechanical Engineering

William M. Tolles
Dean of Science and Engineering

ABSTRACT

New technology was utilized to design and fabricate a self-filtering infrared detector (SFD) optimized for a specific target signature. The SFD was prepared from vacuum deposited, composition-tuned epitaxial films of the semiconductor alloy, PbS_xSe_{1-x}. A filter and detector layer were both grown on opposite sides of a BaF_2 substrate. The detector element was a p-n junction formed by depositing a Pb contact onto a p-type detector layer surrounded by a Au ohmic contact. The optical cuton and cutoff wavelengths were composition-tuned to 4.0 and 5.0 μm by adjusting x in both layers. The measured spectral response of the SFD device was in good agreement with theoretical calculations, whereas, the quantum efficiency was below. The device resistance was two orders of magnitude below the predicted values due to surface leakage. This leakage also caused the peak responsivity and detectivity to be lower than the predicted values. Application of this technology shows great promise provided these problems can be resolved.

TABLE OF CONTENTS

I. INTRODUCTION ---------- 10

A. BACKGROUND ---------- 10

B. THESIS OBJECTIVE ---------- 11

II. ELEMENTARY SEMICONDUCTOR AND INFRARED PHYSICS -- 12

A. GENERAL ---------- 12

B. OPTICAL PROPERTIES ---------- 12

1. The Target and its Signature ---------- 12

2. Optical Properties of Thin Films ------ 13

a. Reflectance ---------- 13

b. Transmittance ---------- 14

c. Absorptance ---------- 14

d. Absorption Coefficient ---------- 15

e. Energy Band Gap ---------- 15

C. ELECTRICAL PROPERTIES ---------- 16

1. Band Theory of Semiconductors and Transport Properties ---------- 16

2. Photo Excitation Process ---------- 18

3. P-N Junction ---------- 19

D. SELF-FILTERING INFRARED DETECTOR DEVICE PROPERTIES ---------- 22

1. Quantum Efficiency ---------- 24

2. Responsivity ---------- 25

3. Noise ---------- 26

a. Thermal (Johnson) Noise ---------- 26

b. Background Noise ---------- 26

4. Detectivity ---------- 27

5. Response Time ---------- 29

III. SELF-FILTERING INFRARED DETECTOR DEVICE MODEL AND PREDICTED PERFORMANCE ---------- 31

IV. SELF-FILTERING INFRARED DETECTOR DEVICE PREPARATION ---------- 34

A. SYNTHESIS OF BULK LEAD SULFIDE ---------- 34

B. EPITAXIAL FILM GROWTH AND EVALUATION ----- 35

1. Film Thickness Evaluation ---------- 36

2. Hall Effect Measurements ---------- 37

3. Schottky Barrier Formation ---------- 37

C. DELINEATION AND MOUNTING ---------- 38

V. SELF-FILTERING INFRARED DETECTOR DEVICE TEST APPARATUS ---------- 39

VI. RESULTS AND DISCUSSION OF DETECTOR PERFORMANCE ---------- 41

A. GENERAL ---------- 41

B. COMPARISON WITH InSb DETECTOR ---------- 42

VII. CONCLUSIONS ---------- 43

VIII. RECOMMENDATIONS FOR FURTHER STUDY ---------- 44

APPENDIX A: NOTATION ---------- 46

TABLES ---------- 48

FIGURES ---------- 49

LIST OF REFERENCES ---------- 62

INITIAL DISTRIBUTION LIST ---------- 64

LIST OF TABLES

I. Self-filtered Infrared Detector Parameters Compared with Commercial InSb Unit ---------- 48

LIST OF FIGURES

1. Idealized Background and Target Spectra ---------- 49

2. PbS_xSe_{1-x} Alloy SFD Device Configuration ---------- 50

3. Energy Bands in a Semiconductor Undergoing the Photo Excitation Process ---------- 51

4. Generation of a Photocurrent in a P-N Junction ---- 52

5. Detector Quantum Efficiency, η_D, and the Spectral Responsivity, R_λ, for the Ideal Detector ---------- 53

6. SFD Device Schematic ---------- 54

7. Transmittance, T, For Various PbS Filter Thicknesses, d_F ---------- 55

8. Net Quantum Efficiency, η, of SFD Device ---------- 56

9. Predicted Spectral Responsivity, R_λ, of SFD Device ---------- 57

10. Predicted Spectral Detectivity, $D^*_{\lambda(J)}$ of SFD Device ---------- 58

11. Schematic Diagram of Apparatus used to grow PbS_xSe_{1-x} With Associated Temperature Profile ----- 59

12. Schematic of the Infrared Detector Testing System ---------- 60

13. The Relative Spectral Responsivity, R_λ (arbitrary units), of Six SFD Device Samples at 77° K ---------- 61

ACKNOWLEDGEMENT

The author would like to express his sincere appreciation to Dr. Allen E. Fuhs and Richard B. Schoolar as thesis co-advisors for their total support, patience, and inspired guidance throughout this project.

The help of several people was essential to affording me the opportunity to do this thesis at the Naval Surface Weapons Center, White Oak Laboratory. In this regard, in addition to my co-advisors, a special thanks goes to CDR Ed Mahon, LCDR Ed Nicholson and Ray Riedl; and to the Air Force Weapons Laboratory, Kirtland AFB, New Mexico, from which research support funds were provided under AFWL #57294 segment number 1133/4.

To its successful completion, a debt of gratitude is owed George Black, Alan Bouley and Steve Foti for their assistance in this project. In addition, the fine typing services of Sarah Tipton and Pam Walker was most appreciated.

I also would like to express sincere thanks to my family for their continued encouragement and support throughout this project.

I. INTRODUCTION

A. BACKGROUND

The Fleet has an urgent need for improved, higher performance infrared detectors for applications in electro-optical seekers for missiles and projectiles. State-of-the-art detectors prepared from InSb single crystals for these systems are made using lengthy, involved procedures, and each device must be individually tested. The combination of low production yield and testing results in very expensive detectors. In addition, the detectors must be used with narrow bandpass optical interference filters to tailor the detector response to a specified spectral region.

A new infrared detector technology has been demonstrated based on PbS_xSe_{1-x} epitaxial films which makes it feasible to incorporate the optical filter in the detector materials [1]. This self-filtering detector, SFD, is easy to fabricate so that its cost, when finally produced commercially, should be significantly less than state-of-the-art InSb detectors.

The SFD is prepared from vacuum deposited, composition-tuned epitaxial films of a chalcogenide semiconductor alloy, PbS_xSe_{1-x}. The filter and detector layers are both grown on BaF_2 substrates. The detector element is a p-n junction formed by depositing a Pb contact onto a p-type detector layer. The optical cuton and cutoff wavelengths can be composition-tuned to any wavelength from 3.9-7 μm by adjusting x in both layers.

B. THESIS OBJECTIVE

The objective of this thesis was to utilize this new technology to design a high performance SFD for a specific target signature and to calculate the required parameters to achieve optimum performance. Once these parameters were obtained, the objective was to prepare a detector optimized on the basis of these parameters and to test the device. These experimental results were compared to the predicted theoretical performance and with the performance of an alternate commercial InSb device.

II. ELEMENTARY SEMICONDUCTOR AND INFRARED PHYSICS

A. GENERAL

It was not intended in this work to relate the detailed theory and derivation of equations which may be found in any text on the subject such as Sze [2]. But, rather it was intended to utilize the pertinent equations that are associated with this unique technology to design an optimum detector for a given target signature.

B. OPTICAL PROPERTIES

1. The Target and its Signature

The term "target" refers collectively to those objects that infrared systems are designed to detect. Although specific details on the radiating characteristics of some targets are classified, reasonably accurate estimates can often be made by applying the radiation laws and certain other information readily available in the open literature. The radiance for a typical missile target whose radiation sources are the skin heating by aerodynamic drag and the rocket plume is as shown in Figure 1 [3]. For a target with a skin temperature of 575° K the peak emission is at λ = 5μm and the plume emission peaks at 4.3μm corresponding to the major CO_2 absorption band.

The target is an infrared source of radiation which will be attenuated as it passes through any part of the earth's atmosphere because the atmosphere is not perfectly transparent. Certain infrared windows exist in the

atmosphere where the attenuation is minimal and, relating to Figure 1, the atmospheric window of closest association is from 3-5 μm (another exists from 8-12 μm). In addition to the target as a source of radiation, other sources which can cause interference are solar and background radiation also shown in Figure 1 [3]. Because most of the target radiation is found between 4-5 μm this band is selected as the best spectral bandpass for the optimum detector. It should be noted that the best spectral bandpass can be determined empirically by associating the anticipated target signature with the nearest atmospheric window, without any great need for complex analytical computations.

2. Optical Properties of Thin Films

Since the SFD is in the form of thin films, expressions developed for thin films must be used to calculate reflectance, transmittance and absorptance of the filter and detector sections. Figure 2 shows the device configuration with an incident photon flux. Reference 4 contains the complex derivations which support the equations related below.

a. Reflectance

The reflectance, R, which is the ratio of reflected radiant flux to incident radiant flux, can be calculated using a function of the refractive indices, N. Referring to Figure 2 where subscript 1 indicates the first medium encountered and subscript 2 indicates the second medium encountered,

$$R = \left[\frac{(N_1 - N_2)}{(N_1 + N_2)}\right]^2 \quad . \tag{1}$$

b. Transmittance

The average transmittance, T, which is the ratio of transmitted radiant flux to incident radiant flux can be calculated from the following expression:

$$T = (1 - R)e^{-\alpha d} , \qquad (2)$$

where α is the absorption coefficient of the medium and d is the thickness of the medium (or film).

c. Absorptance

Absorptance, A, which is the ratio of the absorbed radiant flux to the incident radiant flux can be calculated from,

$$A = 1 - R - T \qquad (3)$$

which, using Equation (2) results in

$$A = (1 - R)[1 - e^{-\alpha d}] \qquad (4)$$

As shown by Zemel, Jensen and Schoolar [5], the refractive index of PbS_xSe_{1-x} at temperature T in the spectral region of interest is represented empirically by:

$$N_{PbS_xSe_{1-x}} \approx 5.2 - 0.7x - 1.3 \times 10^{-3}T \qquad (5)$$

where x is the alloy composition of the thin film medium. The refractive index in air or in a vacuum is unity. The refractive index of the BaF_2 substrate on which the films are deposited is 1.5 [6].

Equations 1, 2, and 3 do not include optical interference effects and yield average values for R, T, and A.

d. Absorption Coefficient

The absorption coefficient, α, is calculated from an empirical expression for both 300° K, room temperature, and 77° K, the boiling point of liquid nitrogen:

(1) at 300° K, α is calculated from the following expression:

$$\alpha = 4.3 \times 10^4 \, (E_\lambda - E_g)^{1/2} cm^{-1} \qquad (6a)$$

where $E_\lambda > E_g + .01$ eV. If $E_\lambda < E_g$, α is calculated as follows:

$$\alpha = 830e^{-66(E_g - E_\lambda)} \; . \qquad (6b)$$

(2) At 77° K, α is determined by:

$$\alpha = 2.5 \times 10^4 \, (E_\lambda - E_g)^{1/2} \text{ for } E_\lambda > E_g + .01\text{eV}. \qquad (7a)$$

If $E_\lambda < E_g$, α is calculated from the following expression:

$$\alpha = 830e^{288(E_\lambda - E_g)} \; . \qquad (7b)$$

The above empirical expressions are the result of work done by Vidyut Prakash [7].

The photon energy E_λ can be converted to wavelength λ using the relation

$$E_\lambda = \frac{hc}{\lambda} \qquad (8)$$

or

$$E_\lambda = \frac{1.24}{\lambda}$$

when E_λ is in units eV and λ is in μm.

e. Energy Band Gap

The energy band gap, E_g, in composition-tuned PbS_xSe_{1-x}, is given by the empirical expression:

$$E_g = .175 + .130x + 4.5 \times 10^{-4} \, (T-77) \qquad (9)$$

which is expressed in units of (eV). The third part of the expression is a correction factor for temperature as reported by Scanlon [8].

It is possible to calculate R, T, and A for a thin film of PbS_xSe_{1-x} using Equations 1-9 provided x, d, and T are known.

C. ELECTRICAL PROPERTIES

1. Band Theory of Semiconductors and Transport Properties

The electron transport in a semiconductor [2] can best be described using the energy band diagram shown in Figure 3. An intrinsic semiconductor is a material in which the allowed charges of the valence electrons form two continuous bands. The valence band is characterized by a maximum allowable energy E_v and the conduction band by a minimum allowable energy E_c, where $E_c > E_V$. At absolute zero, all energy levels in the band below the Fermi energy level E_F will be filled and all those above will be vacant. The separation of these two bands is defined as the energy gap, E_g, which is the difference between E_c and E_v; these energy levels are forbidden to electrons. Electrical conduction occurs when a voltage V is applied to the semiconductor. Electrons in the conduction band spatially drift to +V and the electron voids, or positively charged holes, in the valence band, drift toward -V. The carrier concentrations of electrons and holes is determined by the position of E_F which corresponds to the energy having a probability of electron occupancy of 1/2, as determined by Fermi-Dirac

statistics. The Fermi energy level is at midgap in an intrinsic semiconductor, and the carrier concentrations of electrons and holes are the same, equal to the intrinsic carrier density n_i. If the Fermi level is closer to, E_c, the conduction band edge, the majority of carriers are electrons and the semiconductor is said to be n-type. If the Fermi level is closer to E_v the majority of carriers are holes, and the semiconductor is called p-type. These semiconductors are referred to as extrinsic [2]. If E_F is below E_v or above E_c, the semiconductor is said to be degenerate.

The following relationship, known as the mass-action law, applies to semiconductors

$$P \times n = n_i^2 \quad \text{for a p-type semiconductor} \tag{10a}$$

or

$$N \times p = n_i^2 \quad \text{for an n-type semiconductor} \tag{10b}$$

where P and N are the majority carrier densities and n and p are the minority carrier densities, for p and n-type semiconductors, respectively. The intrinsic carrier concentration, n_i, for a semiconductor is given by the following equation,

$$n_i = 2(2\pi kT/h^2)^{3/2}(m_n^* \times m_p^*)^{3/4} \exp(-E_g/2kT) \tag{11}$$

where m_n^* and m_p^* are the density-of-states effective masses of electrons and holes, respectively, k is Boltzmann's constant and h is Plank's constant [2].

For the density-of-states effective masses for electrons and holes in PbS_xSe_{1-x} we assume

$$m_n^* = m_p^* = \frac{.08\ m_e}{(2-x)} \tag{12}$$

which is a linear interpolation between values reported for PbS and PbSe, where m_e is the electron rest mass [9].

The electrical conductivity σ for n-type material is represented by:

$$\sigma = qN\mu_N + qp\mu_p \tag{13}$$

where q is the electron charge, μ_N is the mobility of electrons, the majority carrier and, μ_p is the mobility of the holes, the minority carrier [2].

For a p-type material the appropriate p and n subscripts would be substituted in the above expression.

2. Photo Excitation Process

An optical photon with energy E_λ can be absorbed and excite an electron across the energy gap, E_g, to create an electron-hole pair as shown at (a) in Figure 3. This can occur if $E_\lambda > E_g$. The electron and hole will, on the average, move through the semiconductor for a distance L_n and L_p, the respective diffusion lengths, before recombining, as shown at (b) in Figure 3. The carrier lifetimes, τ_n and τ_p, are the respective times it takes these processes to occur [2].

The diffusion lengths are calculated from the Einstein relation [2],

$$L = \left(\frac{kT\mu\tau}{q}\right)^{1/2} \tag{14}$$

The subscripts on μ and τ, n for electrons and p for holes, are to be understood.

In PbS_xSe_{1-x} compositions, recent data by Bouley and Schoolar [10] has shown that

$$\tau_n \approx \tau_p \approx 5 \times 10^{-9} \text{ sec.} \quad (15)$$

As Dalvin reported in Ref. 9, the electron mobility, μ_N, is approximately equal to the hole mobility, μ_p, in PbS and PbSe. Assuming a linear variation in μ_N in PbS_xSe_{1-x} with x gives

$$\mu_N = \mu_p = 7.5 \times 10^8 \ (2 - x)T^{-5/2} \ cm^2V^{-1}sec^{-1} \quad (16)$$

where T is in °K.

3. P-N Junction

A photovoltaic detector operates by virtue of a p-n junction formed in the semiconductor. Incident photons produce electron-hole pairs that are, in turn, separated by the electric field at the junction so as to generate a photocurrent or photovoltage. A p-n junction can be formed in a semiconductor by (1) diffusing impurities into a region and converting it from p to n-type, (2) by growth of an n-type epitaxial layer on a p-type semiconductor or (3) in some cases, by depositing a metal of low work-function onto a semiconductor of high electron affinity [2]. In method (3), the junction is also referred to as a Schottky barrier. The associated energy levels, flow of photo excited carriers at (c), and band bending across the p-n junction are shown in Fig. 4.

After the junction is formed, the charge carriers are redistributed and a depletion layer width, W, is formed at the junction. From solutions of Poisson's equation for an abrupt junction [2],

$$W = \left(\frac{2\varepsilon_s (V_{bi}-V)}{qN}\right) 1/2 \qquad (17)$$

where V = applied voltage (bias),

V_{bi} = built-in junction potential, which is the difference in the value of E_F/q in the n and p-type regions, and

ε_s = static dielectric constant.

When a bias, V, is applied to the junction, W decreases as forward bias is applied and increases with reverse bias.

For an abrupt junction, the depletion layer capacitance per unit area $\frac{C}{A}$, is given by [2]

$$\frac{C}{A} = \frac{\varepsilon_s \varepsilon_o}{W} = \left[\frac{q\varepsilon_s \varepsilon_o N}{2(V_{bi} + V)}\right]^{1/2} , \qquad (18)$$

where ε_o is the permittivity of free space.

Values of 175 and 225 have been reported for ε_s of PbS and PbSe, respectively [9]. Assuming a linear variation in the alloy PbS_xSe_{1-x}, ε_s is given by

$$\varepsilon_s = (225 - 50x) \quad . \qquad (19)$$

If a voltage is applied to a junction, current will flow with forward bias but saturates with reverse bias. The current voltage characteristics for the p-n junction are derived on the basis of the following three assumptions as related in Ref. 2:

a. the abrupt depletion-layer approximation, i.e., the built-in potential and applied voltages are supported by a dipole layer with abrupt boundaries, and outside the boundaries the semiconductor is assumed to be neutral.

b. the Boltzmann approximation, i.e., throughout the depletion layer, electrons follow Boltzmann statistics.

c. the low injection assumption, i.e., the injected minority carrier densities are small compared with the majority carrier densities.

From these assumptions the Shockley equation is derived which is the ideal diode law

$$J = J_s(e^{qV/kT}-1) \tag{20}$$

where J_s = saturation current density, J = current density.

The saturation current density due to minority carrier diffusion, J_D is represented by

$$J_D = \frac{qL_p n_i^2}{\tau_p N} + \frac{qL_n n_i^2}{\tau_n P} \quad . \tag{21}$$

The total current density in real diodes also includes current conduction by generation-recombination of electron-hole pairs in the depletion layer and the total saturation current density is

$$J_s = J_D + J_{G-R} \tag{22}$$

The saturation current density corresponding to generation-recombination given by [2]

$$J_{G-R} = \frac{qn_i W}{\tau_{G-R}} \tag{23}$$

where τ_{G-R} is the average time for a generation-recombination process, i.e., an electron-hole pair annihilation in the depletion layer to take place. A value of $\tau_{G-R} = 3 \times 10^{-7}$sec is assumed for PbS_xSe_{1-x} on the basis of recent data on PbS diodes reported by Bouley [10].

For this ideal diode it can be shown by taking the derivative of Equation 20 that the resistance-area product RA with zero bias is represented by

$$RA = \frac{kT}{qJ_s} \tag{24}$$

where R is the junction zero-bias resistance for a specific band gap, E_g, and operating temperature.

For the PbS_xSe_{1-x} alloy system it has been shown that

$$RA = 2.7 \times 10^{-4} e^{\frac{qE_g}{2kT}} \tag{25}$$

for a specific band gap, E_g, and operating temperature, T, [10].

If the exponent in Equation 25 < 13, current is predominantly due to diffusion.

If the exponent > 13, current is predominantly due to generation-recombination [10].

D. SELF-FILTERING INFRARED DETECTOR DEVICE PROPERTIES

The technical literature abounds with a wide variety of connotations for the word "detector". It is used to refer to a demodulator, to an indicator of a null balance condition in a bridge circuit, to a mixer in a superheterodyne receiver, or to a device indicating the presence of almost any physical entity, such as radiant energy. For this latter technology, an infrared detector is simply a transducer of electromagnetic radiant energy with photon wavelengths ranging from .7 - 100 μm. It converts photon energy into some other measurable form, usually electrical.

It is convenient to group IR detectors into two classes that differ by the physical mechanism involved in the

detection process. In one group, called "thermal detectors", the heating effect of the incident radiation causes a change in some electrical or mechanical property of the detector. In the other group, called "photon" or "quantum detectors", there is a direct interaction between the incident photons and the electrons of the detector material. Therefore, the response of a thermal detector is proportional to the energy absorbed, whereas that of a photon detector is proportional to the number of photons absorbed.

In general, the photon detector is preferred because it has better sensitivity and higher operating frequencies than the thermal type. In addition, photon detectors are sensitive to the spectral content of the incident radiation, whereas thermal detectors are not.

The signal to noise ratio of the photon detector can be greatly enhanced if the detector spectral response is matched to the spectral emission of a target. This can be done with the self-filtering infrared detector (SFD) described in this report. This detector is prepared from two thin layers of the semiconductor alloy PbS_xSe_{1-x}. One layer filters undesired radiation at wavelengths below λ_F and the second layer is made into a photovoltaic detector which is sensitive to some longer wavelength λ_D. Both λ_F and λ_D can be adjusted to any wavelength in the spectrum between 3-7 μm. In this section, mathematical expressions are developed which are needed to model the performance of a SFD prepared from PbS_xSe_{1-x}.

1. Quantum Efficiency

Total or net quantum efficiency, η, is the number of charge carriers produced and collected per incident photon and is a function of wavelength

$$\eta = \frac{N_\lambda}{\phi} \quad , \tag{26}$$

where N_λ = number of photo excited current carriers of wavelength λ collected per second per unit detector area and ϕ = incident photon flux on the detector layer.

Referring to Figure 2, the SFD contains a filter layer with transmittance T_F and a detector layer with a quantum efficiency η_D.

The resulting device quantum efficiency is given by

$$\eta = T_F \eta_D \quad . \tag{27}$$

Now from classical optics,

$$T_F = (1 - R_F) e^{-\alpha_F d_F} \quad , \tag{28}$$

where R_F = reflectance loss term at the filter layer, α_F = thickness of the filter layer.

The efficiency of the detector section can be calculated using the equations [11]

$$\eta_D = (1 - R_D) e^{-\alpha_D (d_D - L_n)} [1 - e^{-2\alpha_D L_n}] \text{ for } L_n < d_D, \tag{29a}$$

$$\eta_D = (1 - R_D) [1 - e^{-2\alpha_D d_D}] \text{ for } L_n > d_D \quad , \tag{29b}$$

where the subscripts now refer to the detector layer and L_n = minority carrier diffusion length.

Since the detector film interfaces with a Pb contact, its internal reflectance is essentially unity or 100% reflection. Because of this, the effective thickness of the

region which absorbs and diffuses carriers to the junction is 2L and Equation 29 is modified accordingly.

Therefore, combining Equations 28 and 29, the device quantum efficiency is expressed as

$$\eta = (1 - R_F)e^{-\alpha_F d_F}(1 - R_D)e^{-\alpha_d}(d_D - L_n)[1 - e^{-2\alpha_d L_n}]. \quad (30)$$

The above relationships are good to a first order approximation. Second order effects are considered minimal and are neglected.

Utilizing the equations previously presented, the total or net quantum efficiency, η, can be calculated for any PbS_xSe_{1-x} SFD.

Quantum efficiency for the ideal photon detector in relation to wavelength is shown in Figure 5.

2. Responsivity

One of the simplest descriptions of detector performance is its spectral responsivity, R_λ, the detector voltage output per unit photon power input.

In a p-n junction,

$$R_{\lambda\,(A/W)} = \frac{N_\lambda q}{\phi E_\lambda} = \frac{\eta q}{E_\lambda} \quad , \quad (31)$$

where E_λ is the photon energy and the units of R_λ are amps per watt. This is the responsivity for a short circuit p-n junction current. For the open circuit voltage responsivity,

$$R_{\lambda\,(V/W)} = R_{\lambda\,(A/W)}\ R = \frac{\eta q R}{E_\lambda} \quad (32)$$

where R is the junction or SFD device resistance.

Responsivity in relation to wavelength for an ideal photon detector is also shown in Figure 5.

3. Noise

In an infrared system, as in any information-transmitting system, spontaneous electrical fluctuations that are called "noise" impose the ultimate limit on the transmission of information. Hence an understanding of noise is essential to an understanding of the limitations imposed on the performance of an infrared system. In its broadest sense the term "noise" refers to any spurious or unwanted signals in a system. Here, we are not only interested in the random electrical fluctuations generated in circuit elements but also in externally generated effects.

The two fundamental sources of electrical noise in a junction device are generated by internal thermal fluctuations and background photon fluctuations [12].

a. Thermal (Johnson) Noise

The noise current due to random thermal fluctuations of the charge carriers is given by

$$i_J = \left(\frac{4kT\Delta f}{R}\right)^{1/2} \tag{33}$$

where Δf = electrical bandwidth of the associated circuit. From Ohm's Law, the voltage due to thermal or Johnson noise is

$$V_J = (4kT\Delta fR)^{1/2} \quad . \tag{34}$$

In a well-prepared detector, Johnson noise will be the predominant noise source neglecting background noise.

b. Background Noise

When a detector is exposed to radiation from a background with a temperature, T_B, the background noise,

i_{BLIP}, (BLIP means Background Limited Infrared Photodetector) is expressed by

$$i_{BLIP} = q(\overline{2\Delta N}^2\ \eta A\Delta f)^{1/2} \qquad (35)$$

where A = area of the detector, $\overline{\Delta N}^2$ = the average background photon flux for a given T_B. For an ideal photon detector with a sharp wavelength cutoff at λ_c, the background photon flux can be expressed by [3]

$$\overline{\Delta N}^2 = 2\pi c\ (\frac{kT_B}{hc})e^{-\frac{hc}{kT_B}}\ \frac{1}{\lambda c}\ [2(\frac{kT_B}{hc})^2 + 2(\frac{kT_B}{hc})(\frac{1}{\lambda c}) + \frac{1}{\lambda_c^2}] \qquad (36)$$

where λ_c = cutoff wavelength, c = speed of light, h = Planck's constant.

From Ohm's Law, the noise voltage due to background is

$$V_{BLIP} = Rq(2\overline{\Delta N}^2\ \eta A\Delta f)^{1/2}. \qquad (37)$$

4. Detectivity

The most important figure of merit parameter for a detector is its detectivity, D_λ^*, pronounced "dee-star" and the units are $cm(Hz)^{1/2}W^{-1}$ when A is measured in cm^2 and Δf is in Hz. A convenient way to remember D_λ^* is that it is the signal-to-noise ratio when one watt is incident on a detector having a sensitive area of 1 cm^2 and the noise is measured with an electrical bandwidth of 1 Hz. Thus D_λ^* is a normalized detectivity that is particularly convenient for comparing the performance of detectors with different areas when used in circuits having different bandwidths. The expression for D_λ^* is as follows [13]

$$D_\lambda^* = \frac{R_\lambda(V/W)A^{1/2}\Delta f^{1/2}}{V_N} \qquad (38)$$

where V_N = measured noise voltage.

For a Johnson noise limited detector, where V_N is assumed to be only Johnson noise,

$$D^*_{\lambda(J)} = \frac{q\eta(RA)^{1/2}}{2E_\lambda(kT)^{1/2}} \quad . \tag{39}$$

Therefore, the upper limit of achievable detectivity can be calculated for an operating device of given parameters at any T.

When a device is used with high background radiation the detectivity will be background limited. $D^*_{\lambda(BLIP)}$ can be expressed by

$$D^*_{\lambda(BLIP)} = \frac{R_\lambda(V/W)A^{1/2}\Delta f^{1/2}}{V_{BLIP}} \tag{40}$$

where V_{BLIP} = background induced noise voltage. Using equation 37 yields

$$D^*_{\lambda(BLIP)} = \frac{\eta^{1/2}}{E_\lambda(2\overline{\Delta N^2})^{1/2}} \tag{41}$$

where E_λ = photon energy in Joules. The above expression assumes the detector has a 180° cone angle field of view (i.e., a full hemisphere).

As the cone angle is collapsed to reduce the background exposed to the detector, the expression for $D^*_{\lambda(BLIP)}$ is as follows

$$D^*_{\lambda(BLIP)} = \frac{\eta^{1/2}}{[E_\lambda(2\overline{\Delta N^2})^{1/2}][\sin(\frac{\theta}{2})]} \tag{42}$$

where θ = cone angle.

For a more efficient device, the resistance-area (RA) product should be made as high as possible so $D^*_{\lambda(J)}$ is high and actually greater than $D^*_{\lambda(BLIP)}$. Then $D^*_{\lambda(BLIP)}$ can be

increased by cold-shielding the detector which will yield the highest attainable performance.

As already mentioned cold-shielding can be accomplished by decreasing the detector solid cone angle to eliminate background noise. A second way to further cold-shield is with a spectral filter, i.e., to filter out the undesirable wavelengths.

5. Response Time

The response time of a detector is characterized by its "responsive time constant", the time that it takes for the detector output to reach $(1 - \frac{1}{e})$, i.e., 63%, of its final value after a sudden change in irradiance. It is worthy to note this definition is identical to that used to describe the charge or discharge of an RL circuit or RC circuit [13].

The response time, τ_c, can be limited by transit time, i.e., the time it takes the current to cross the p-n junction. It can also be limited by the resistance-capacitance, RC, time constant characteristic of the device.

The transit time for a photo excited electron is represented by

$$\tau_c = \frac{W}{L_n/\tau_n} \quad ,$$

and using Equation 14,

$$\tau_c = \frac{W}{\left(\frac{kT\ \mu_n}{q\tau_n}\right)1/2} \tag{43}$$

where μ_n = mobility of the excited electron and τ_n = excited electron (minority carrier) lifetime. The transit time for

PbS_xSe_{1-x} is estimated to be on the order of 10^{-12} sec and is therefore negligible in comparison to the RC time constant.

The RC time constant can be represented by

$$\tau_{RC} = R\,C = (RA)\left(\frac{C}{A}\right)$$

Using the capacitance-area relationship, Equation 18, and Equation 25, the resistance-area product relationship, yields

$$\tau_{RC} = 2.7 \times 10^{-4}\, e^{\frac{qE_g}{kT}} \left[\frac{q\varepsilon_s N}{2(V_{bi} \pm V)}\right]^{1/2} . \qquad (44)$$

The cutoff frequency, f_c, defined as the frequency at which power is one half the peak value due to clipping is given by

$$f_c = \frac{1}{2\pi\tau_{RC}} . \qquad (45)$$

III. SELF-FILTERING INFRARED DETECTOR DEVICE MODEL AND PREDICTED PERFORMANCE

A schematic diagram of the self-filtering device (SFD) is shown in Figure 2. Figure 6 shows a bottom view of the detector and a side view of the cryotip on which it is mounted with the dimensions as shown.

The filter section of the device must have a sharp cuton for λ = 4.0 μm which from Equation 8 corresponds to an energy gap of .31 eV. Inserting this value for E_g, and an operating temperature T = 77° K, into Equation 9 and solving for x yields x = 1.0. This indicates that a pure PbS filter should provide the required sharp cuton of 4.0 μm at the desired operating temperature of 77° K.

In a similar manner, the detector composition is determined using Equations 8 and 9. The photon energy at the required 5 μm cutoff corresponds to an energy gap of .248 eV. A detector will cutoff at this wavelength provided that E_g = .248 eV. From Equation 9 this will occur in PbS_xSe_{1-x} at an operating temperature of 77° K when x = 0.60. Therefore, the filter layer must be pure PbS and the detector must be a $PbS_{.6}Se_{.4}$ layer in order to have the required spectral bandpass response.

The transmission of three PbS filter layers of varying thickness of $d_F = 5 \times 10^{-4}$cm, 10×10^{-4}cm, and 15×10^{-4}cm are calculated using Equations 7a and 7b and are shown in Figure 7. R_F is calculated from Equation 1 and found to be

0.396 where $N_1 = 1.0$ and $N_2 = 4.4$, where N_2 was computed using Equation 5.

For the device detector layer, $d_F = 10$ μm is chosen because this thickness provides adequate attenuation at short wavelengths to block solar interference. Figure 8 shows a plot of the predicted net quantum efficiency of the SFD with $d_f = 10$ μm and $d_D = 2$ μm arrived at using equations previously developed.

From Equation 14 a value of 8.19×10^{-4} cm is computed for the minority carrier diffusion length, L_n. From Equation 16 the carrier mobility, μ_n, is computed to be 2.02×10^4 $cm^2\ V^{-1}\ sec^{-1}$. Reflectance, R_D, of 0.265 is computed from Equation 1 for $N_1 = 1.5$ and $N_2 = 4.68$, where N_2 was computed using Equation 5. The detector absorption coefficient, α_D, is calculated from Equations 7a and 7b for the varying values of E_λ, the incident photon energy. Pertinent values are substituted into Equations 29a and 29b to give, η_D, the quantum efficiency of the detector. The filter transmission T_F, and the detector efficiency, η_D, are combined in Equation 27 to yield the total or net quantum efficiency for the device, η, which is shown in Figure 8.

The resistance-area product computed from Equation 25 is $5.05 \times 10^4 \Omega cm^2$. For a detector area, $A = 3.2 \times 10^{-2} cm^2$, the resistance is $1.58 \times 10^6 \Omega$.

The spectral responsivity, R_λ, calculated from Equation 31 is shown graphically in Figure 9.

It is assumed the device is Johnson noise limited and the Johnson noise limited spectral detectivity, $D^*_{\lambda(J)}$ is

calculated from Equation 39 and is shown graphically in Figure 10. A peak $D^*_{\lambda(J)}$ of 6.0×10^{12} $\frac{cmHz^{1/2}}{W}$ is predicted at $\lambda = 4.8$ μm. This is much higher than the background limited value which is the desired condition as previously stated.

IV. SELF-FILTERING INFRARED DETECTOR DEVICE PREPARATION

A. SYNTHESIS OF BULK LEAD SULFIDE

As contained in Ref. 14, lead sulfide ingots were prepared by reacting 99.9999% pure lead and sulfur in sealed evacuated quartz ampoules. The elements were carefully weighed into 100 gm charges, 0.01% atomically rich in sulfur. The quartz tube was cleaned in HF, rinsed in distilled water, evacuated to 10^{-6} Torr, and baked out with a torch. The oxide was removed from the lead by melting it in the ampoule under a partial pressure of hydrogen. After cooling to room temperature, the ampoule was loaded with the sulfur charge, evacuated to 10^{-6} Torr and sealed off. The lead and sulfur were then reacted with a torch. This step must be done with great care since the reaction is exothermic. The coldest part of the ampoule must be kept below 500° C otherwise the vapor pressure of the pure sulfur will become dangerously high. After the reaction appeared complete, the ampoule was placed into a 1200° C furnace and annealed for 48 hours. This last step insured complete reaction of the element.

A similar procedure was carried out to synthesize $PbS_{.6}Se_{.4}$. The only difference is that from their respective molecular weights, the correct amounts of Pb, S and Se are computed to give the stoichiometrically correct compound $PbS_{.6}Se_{.4}$.

B. EPITAXIAL FILM GROWTH AND EVALUATION

Lead sulfide films were epitaxially grown by vacuum sublimation of the materials described in the previous section onto heated BaF_2 substrates. The vacuum system was a standard oil diffusion pump, liquid nitrogen trapped, 6 in bell-jar evaporator. The PbS_xSe_{1-x} was contained in the outer cavity of a dual chamber quartz crucible which was placed concentrically within the coiled furnace windings inside the bell-jar. The inner cavity extended below the outer chamber and was not within the furnace windings. A schematic of the furnace is shown in Figure 11.

The procedure for film growth was as follows; approximately 20 gm of a PbS ingot was pulverized with a mortar and pestle and loaded into the quartz crucible. Freshly cleaved BaF_2 substrates, approximately 1 mm thick and 15 mm square, were supported by the substrate holders. The BaF_2 substrates were cleaved in air along the <111> cleavage plane just prior to placement in the vacuum chamber. The system was evacuated to 1×10^{-6} Torr.

The substrate was heated to 450° C; the quartz crucible was baked out at 450° C for 10 minutes and, when the correct furnace temperature profile was attained as shown in Figure 11, a shutter in front of the substrate was opened. The power setting to the furnace was adjusted so that film deposition, rates were approximately 2 μm/hr. At the end of deposition, the shutter was closed, the furnace and substrate heater were turned off, and the substrate was cooled to room temperature under vacuum [14].

The detector structure is prepared in two steps. First the filter layer is grown; after brief storage at atmospheric conditions, the substrate is flipped over and the detector layer is grown on the opposite side using the appropriate charge. In our case, PbS was used for the filter and $PbS_{.6}Se_{.4}$ was used for the detector layer.

There was also a substrate heater to control the upper end of the temperature profile.

When the detector layer is grown it is essential that the film is p-type to obtain the p-n junction with a lead contact. A small amount of a Group VI chalcogenide usually S or Se is present in the central cavity of the quartz crucible to insure the material will be p-type. An excess of Pb will produce an n-type material.

When the detector layer was grown, 100 mg of sulfur was placed in the inner cavity of the quartz crucible as shown in Figure 11. This extra sulfur was co-evaporated with $PbS_{.6}Se_{.4}$ to ensure that the deposited film was p-type. Maintaining the inner cavity at room temperature yielded p-type layers with $p = 5 \times 10^{17} cm^{-3}$ due to the high vapor pressure of sulfur.

1. Film Thickness Evaluation

The film thickness was determined from analysis of interference fringes appearing in infrared transmittance patterns. The transmitted infrared radiation was varied between 2.0 and 15.0 μm using a Perkin Elmer Model 21 Spectrometer. The thickness d was determined using the

familiar Bragg equation

$$m\lambda_m = 2Nd \tag{46}$$

where m = the order of interference fringe (integer for transmittance maxima), λ_m = the wavelength of the mth maximum, N = the refractive index.

The order m was determined by taking the ratio of the wavelengths of two consecutive fringes and finding the corresponding ratio of two consecutive integers.

2. Hall Effect Measurements

Hall effect and electrical resistivity, ρ, measurements were made on all films grown to determine their Hall coefficient, R_H, mobility and carrier concentration determined from [2]

$$R_H = \frac{V_H}{I_s}\ \frac{d}{B} \tag{47}$$

$$\rho = \frac{R'wd}{\ell} \tag{48}$$

$$\mu = \frac{R_H}{\rho} \tag{49}$$

and,

$$N = \left|\frac{1}{qR_H}\right| \tag{50}$$

where V_H = Hall voltage, I_s = sample current, B = magnetic field, w = sample width, ℓ = sample length, R' = Hall sample resistance.

3. Schottky Barrier Formation

Schottky barriers were formed by depositing 99.9999% pure lead through a stainless-steel mask that delineated arrays of six circular elements on the PbS_xSe_{1-x} films. Each element was of area $3.2 \times 10^{-2} cm^2$.

C. DELINEATION AND MOUNTING

These detector elements are prepared in a separate 18 inch multi-turret vacuum chamber equipped with a rotatable sample holder. The sample was placed in the sample holder, detector layer side facing down. This system was evacuated to 1×10^{-7} Torr and the sample was vacuum annealed above the first turret at 170° C for 30 minutes to desorb any surface oxide layers. It was then cooled to room temperature, still under vacuum, and was rotated to another turret where the sample holder was placed on a stainless steel mask with an array of six circular openings of diameter 2.032 mm. The Pb contacts were approximately 1 μm thick [14].

The sample holder was then rotated to another turret and placed over a different stainless steel mask with openings which delineate the locations of Au electrical contacts evaporated in relation to the lead contacts as shown in Figure 6.

The sample was then removed from the system and was sliced into six individual elements which were trimmed by hand. This process yields six devices each as shown in Figure 6.

One of the devices was bonded to the cryotip with silver epoxy. The central Pb contact and circular Au ohmic contact were epoxied to copper foils insulated from the copper cryotip. These, in turn, were bonded to two wires that lead out from the cryotip to the system preamp. When completed, the device was ready for testing.

V. SELF-FILTERING INFRARED DETECTOR DEVICE TEST APPARATUS

SFD devices were tested for performance utilizing the apparatus as shown in Figure 12. The quantities needed to calculate the absolute responsivity, R_λ, and detectivity, D^*_λ of a detector are: the signal and noise voltages, V_s and V_n, the equivalent noise bandwidth of the measuring circuit, Δf, the area of the detector, A, and the irradiance, ϕ, (radiant photon flux incident per unit area) from a calibrated blackbody source, and the relative spectral response [13].

The test apparatus consists of a blackbody source and blackbody temperature controller which provided a calibrated source of infrared radiation. All measurements were made at a blackbody temperature of 506° K with the sample cooled to 77° K. The limiting apertures were used to provide an accurately known radiation flux from the blackbody. The variable-speed chopper provided a constant frequency 510 Hz square wave-signal of the radiant energy. The preamplifier was utilized to boost the detector signal which is then measured by the wave analyzer at the chopping frequency of 510 Hz.

This basic test set as described above was used to measure the detector response to the blackbody source.

The relative spectral response of the detector was measured by rotating the detector into the optical path of a monochromator. In essence, the spectral-response test set provides radiant flux in a very narrow spectral band

centered about any desired wavelength between 3 and 12 μm and compares the response of the detector under test with that of a reference thermocouple detector that responds equally to energies at all wavelengths.

The monochromator and reference detector are the heart of the spectral response test set. The beam from the monochromator falls on a movable plane mirror. The reflected and transmitted portions of this beam travel, respectively, to the reference detector and the detector under test. The output of both are read and the relative spectral response was computed by taking the ratio of detector output to reference output.

VI. RESULTS AND DISCUSSION OF DETECTOR PERFORMANCE

A. GENERAL

The relative responsivities of the six SFD devices are shown in Figure 13. They each manifested the required spectral sensitivity. Filter cutoff (detector cuton) occurred at approximately 4.0 μm and detector cutoff occurred at approximately 5.0 μm as predicted. The dip in each responsivity plot in Figure 13 was caused by CO_2 absorption at 4.26 μm in the test instrument and was not due to the detector. The small variations in detector cutoff from sample to sample was due to minor variations in the composition-tuning variable x which was caused by dissociation of source material during film growth.

The peak values of responsivity, $R_{\lambda p}$, are all listed in Table I along with device resistance, R, peak detectivity, $D^*_{\lambda p}$, net quantum efficiency, η, and filter cutoff (detector cuton), λ_F, and detector cutoff, λ_D.

Peak responsivities were below the predicted values. This was primarily due to the low resistances of the samples. Further testing and analysis of the temperature dependence of the diode conduction [15] showed that the leakage was due to conduction through a surface oxide layer [16] within the small spacing between the Pb contact and concentric Au ohmic contact.

The peak quantum efficiencies were also below the predicted values. This in turn resulted in values of peak D^*_λ which were lower than the theoretical values.

B. COMPARISON WITH InSb DETECTOR

In comparison with the InSb unit the SFD devices had the required spectral sensitivity, but had lower quantum efficiencies and lower peak detectivities. Therefore, by this comparison, additional development work is required on the SFD devices before they will be competitive with the InSb units. The theoretically predicted results indicate the potential for an improved, competitive detector exists in this technology.

VII. CONCLUSIONS

This study led to the following conclusions:

1. The theoretically predicted results indicate the potential for an improved competitive detector exists in this technology.
2. SFD device samples are not yet far enough in development to be engineered into Navy systems.
3. Surface current leakage was caused by proximity of the Pb Schottky contact to the Au ohmic contact which resulted in lower device performance.
4. When further developed, these sensors offer a number of advantages over commercial detectors:
    a). They should have higher detectivities,
    b). higher operating temperatures, and
    c). are expected to be cheaper to produce.
5. Future applications of this technology are considered feasible in the following areas:
    a). Laser receivers
    b). Rocket plume detectors
    c). Multicolor sensors.

VIII. RECOMMENDATIONS FOR FURTHER STUDY

Additional study in the following areas could greatly effect progress and advancement in this new technology:

1. The net quantum efficiencies of the SFD samples were lower than predicted values based on previous measurements on smaller samples. In order to understand this anomaly, it is recommended that the sensitivity contour of the larger SFD samples be measured with a high-resolution laser spot scanner to determine if there are nonuniformities, such as dead spots. If nonuniformities are observed, techniques should be developed to produce uniformly sensitive devices.

2. Based on leakage measurements, sample resistances were significantly less than predicted due to surface leakage. In order to improve the SFD device resistance it is recommended that the effects of surface leakage be minimized. It is believed this can be done in two ways, and it is recommended each be explored:

   a. Changing the contact geometry so that the Au ohmic contact is shifted away from the Pb Schottky contact. This in effect would reduce the conduction path for surface leakage.

   b. Eliminating the surface oxide on the samples. One technique which has been investigated and showed promise in a similar circumstance is through surface passivation with an overcoating of As_2S_3 [16]. This technique should be applied to the SFD devices.

3. Development of a computer model for the equations and procedures necessary to design and test a SFD device would be helpful in advancing this technology. This should include computer plotting of the pertinent data.

APPENDIX A

NOTATION

A (cm^2)	Sample area
A (dimensionless)	Optical absorptance
B (Webers m^{-2})	Magnetic field
$c = 3.0 \times 10^{10}$ (cm sec^{-1})	Velocity of light
D^*_λ (cm $Hz^{1/2} W^{-1}$)	Spectral detectivity
d (cm)	Sample thickness
E_g (eV)	Direct energy gap
E_λ (eV) or (J)	Photon energy
f (Hz)	Frequency
Δf (Hz)	Frequency bandwidth or equivalent noise bandwidth
$h = 6.63 \times 10^{-34}$ (J sec)	Planck's constant
I_s (A)	Sample current
$k = 1.38 \times 10^{-23}$ (J K^{-1})	Boltzmann constant
L (cm)	Minority carrier diffusion length
ℓ (cm)	Sample length
$m_o = 9.1 \times 10^{-31}$ (kg)	Electron mass
m^* (gm)	Average carrier effective masses
N_λ (sec^{-1} cm^{-2})	Photo excited current carriers
N, P (cm^{-3})	Majority carrier concentration
n, p (cm^{-3})	Minority carrier concentration
N (dimensionless)	Refractive index
$\overline{\Delta N}^2$ (sec^{-1} cm^{-2})	Total background photon flux for a given temperature

$q = 1.60 \times 10^{-19}$ (Coul)	Electron charge
R (ohm)	SFD device (or junction) resistance
R' (ohm)	Hall sample resistance
R_H (m^3 $Coul^{-1}$)	Hall coefficient
R_λ (VW^{-1})	Spectral responsivity
$\mathcal{R}$ (dimensionless)	Optical reflectance
T(°K)	Temperature
$\mathcal{T}$ (dimensionless)	Optical transmittance
V (V)	Applied voltage (bias)
V_{bi} (V)	Built in potential of a junction or barrier
V_H (V)	Hall voltage
W (cm)	Depletion layer width
w (cm)	Sample width
α (cm^{-1})	Optical absorption coefficient
$\varepsilon_o = 8.85 \times 10^{-14}$ (F cm^{-1})	Permittivity of free space
ε_s (unitless)	Static dielectric constant
λ (μm)	Photon wavelength
η (dimensionless)	Quantum efficiency
ϕ (sec^{-1} cm^{-2})	Photon flux (irradiance)
ρ (ohm-cm)	Resistivity
τ_c (sec)	Response time (time constant)
$\tau_{n,p}$ (sec)	Minority carrier lifetime
μ ($cm^2V^{-1}sec^{-1}$)	Carrier mobility

TABLE I

Self-filtered infrared detector parameters compared with commercial filtered InSb unit.

Sample Device Identification	Filter Cutoff (Detector Cuton) $\lambda_F(\mu m)$	Detector Cutoff $\lambda_D(\mu m)$	Peak Responsivity $R_{\lambda p}(V/W)$	Resistance $R(\Omega)$	Peak Detectivity $D^*_{\lambda p}(\frac{cmHz^{1/2}}{W})$	Net Quantum Efficiency $\eta(\%)$
Predicted-Theoretical	4.0	5.0	1.5×10^6	1.58×10^6	6.0×10^{12}	40.0
Filtered InSb[a]	3.95	4.75	2.0×10^5	1.0×10^5	1.3×10^{11}	56.0
PbS_xSe_{1-x}						
52	4.30	4.73	144	800	3.43×10^{10}	4.9
58	3.95	4.63	166	338	2.29×10^{10}	14.2
61	3.95	4.95	142	625	1.45×10^{10}	6.1
63	3.95	4.8	166	556	1.69×10^{10}	8.6
64	3.95	4.80	191	1250	1.95×10^{10}	4.1
65	3.98	4.73	114	165	9.1×10^9	19.0

a. Manufactured by Santa Barbara Research Center, Goleta, CA

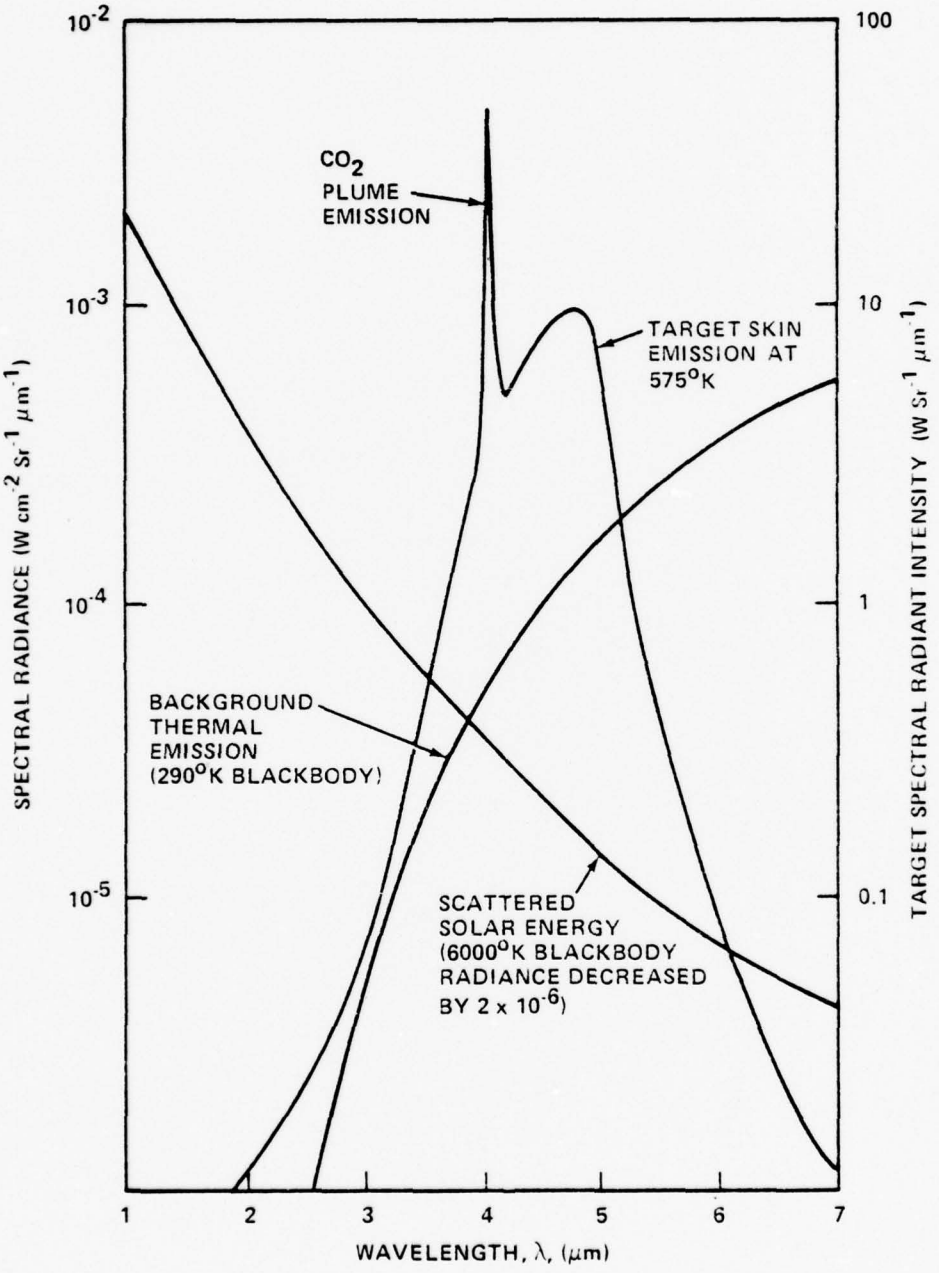

FIGURE 1. IDEALIZED BACKGROUND AND TARGET SPECTRA

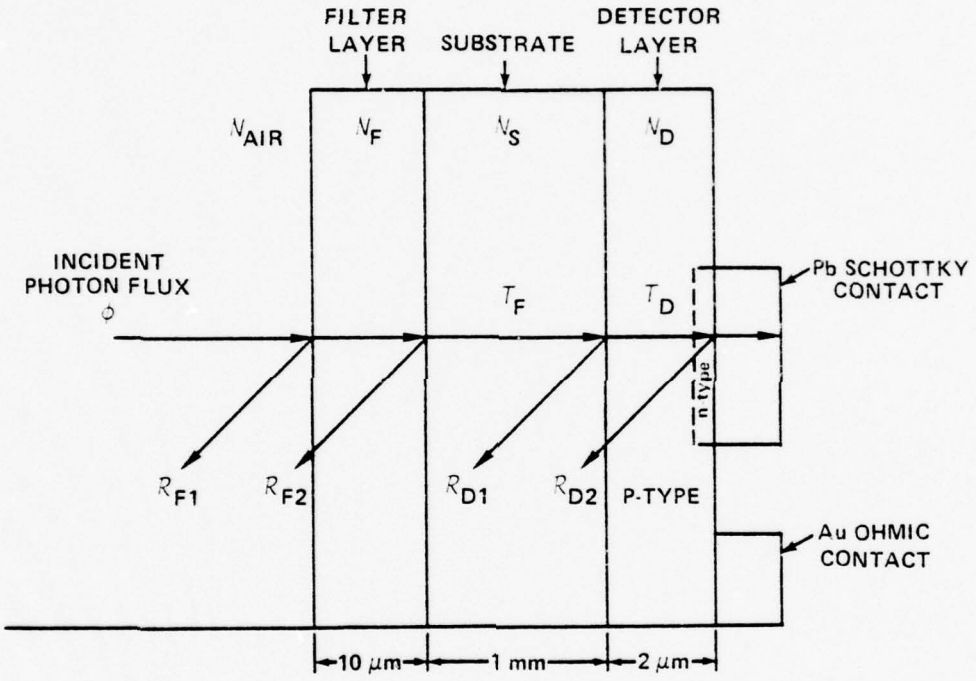

FIGURE 2. Pb S_x Se_{1-x} ALLOY SFD DEVICE CONFIGURATION

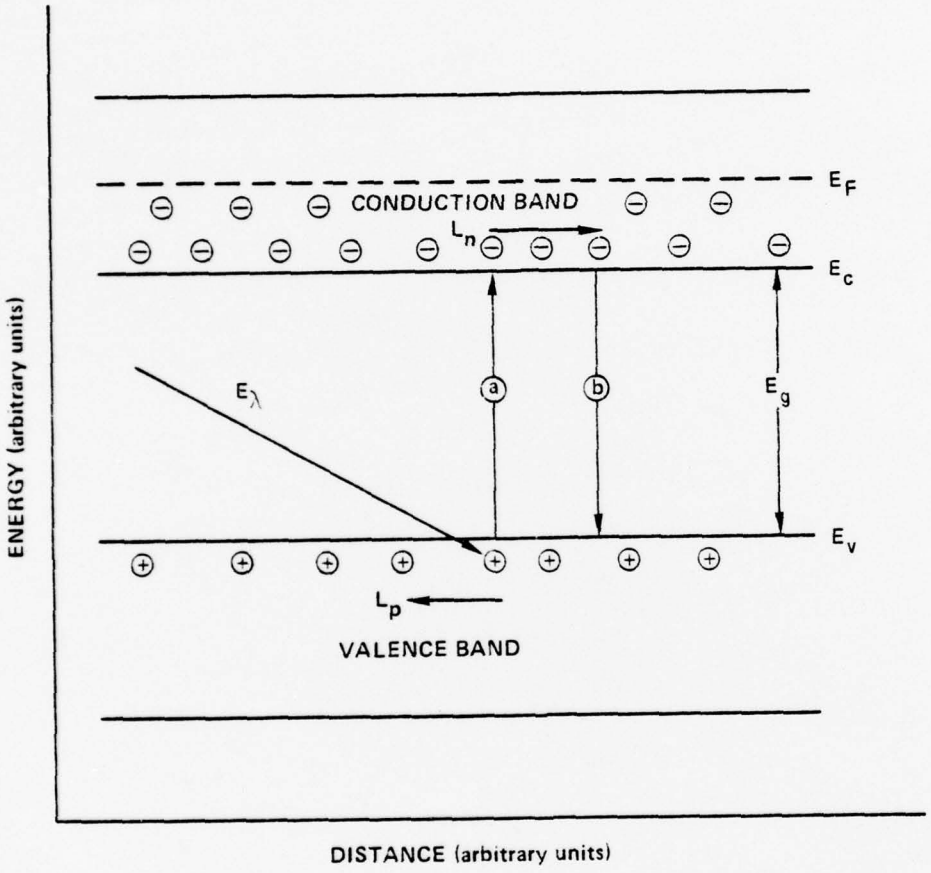

FIGURE 3. ENERGY BANDS IN A SEMICONDUCTOR
UNDERGOING THE PHOTO EXCITATION PROCESS

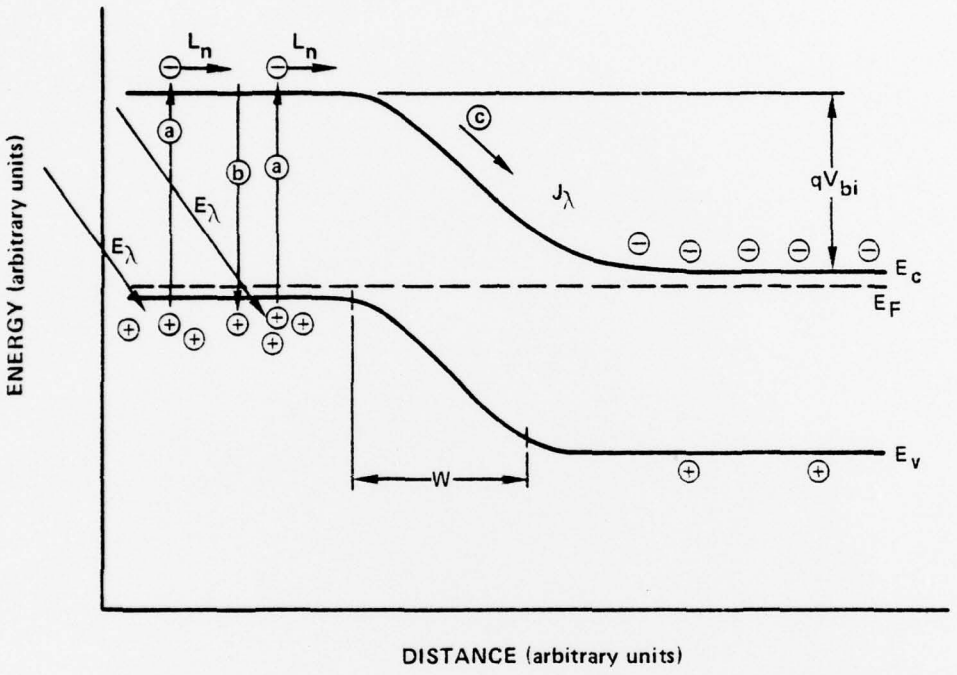

FIGURE 4. GENERATION OF A PHOTOCURRENT IN A P-N JUNCTION

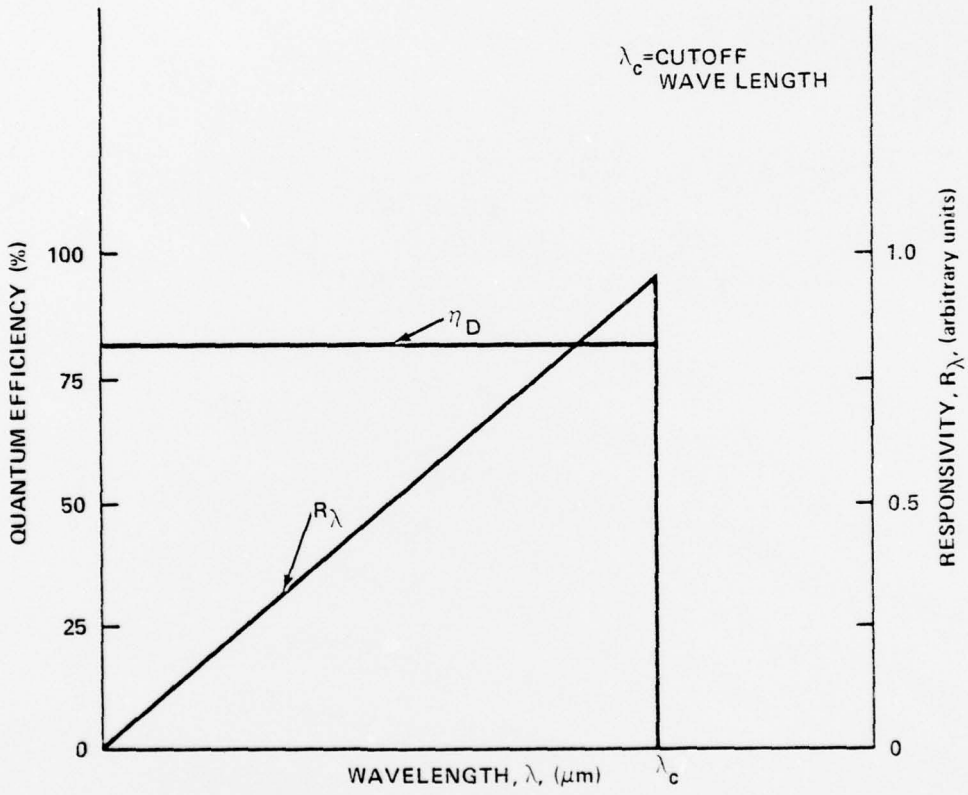

FIGURE 5. DETECTOR QUANTUM EFFICIENCY, η_D, AND THE SPECTRAL RESPONSIVITY, R_λ, FOR THE IDEAL DETECTOR

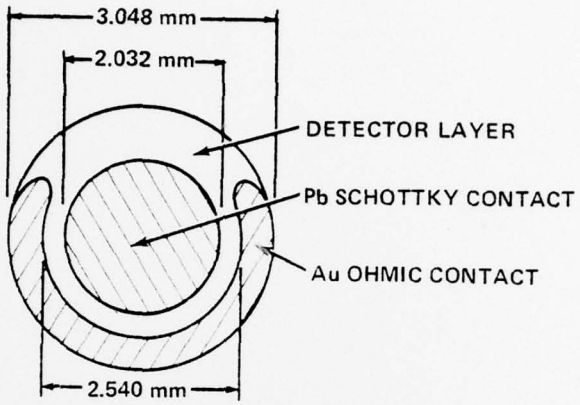

BOTTOM VIEW (DETECTOR SIDE)

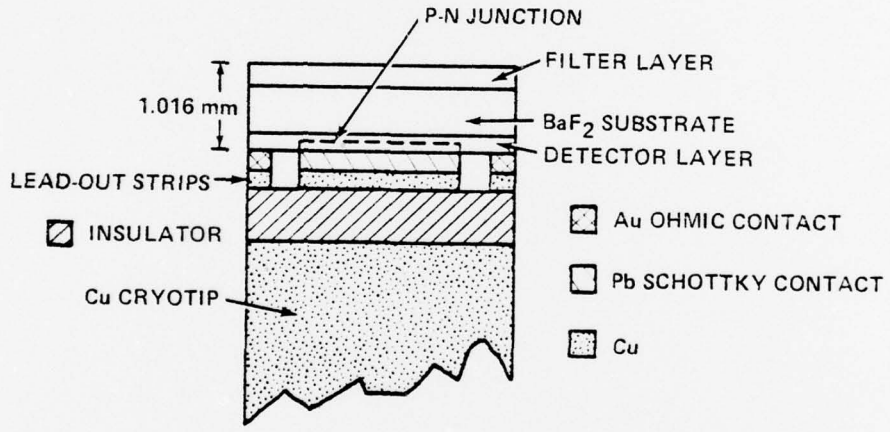

SIDE VIEW OF DETECTOR AFFIXED TO Cu CRYOTIP

FIGURE 6. SFD DEVICE SCHEMATIC

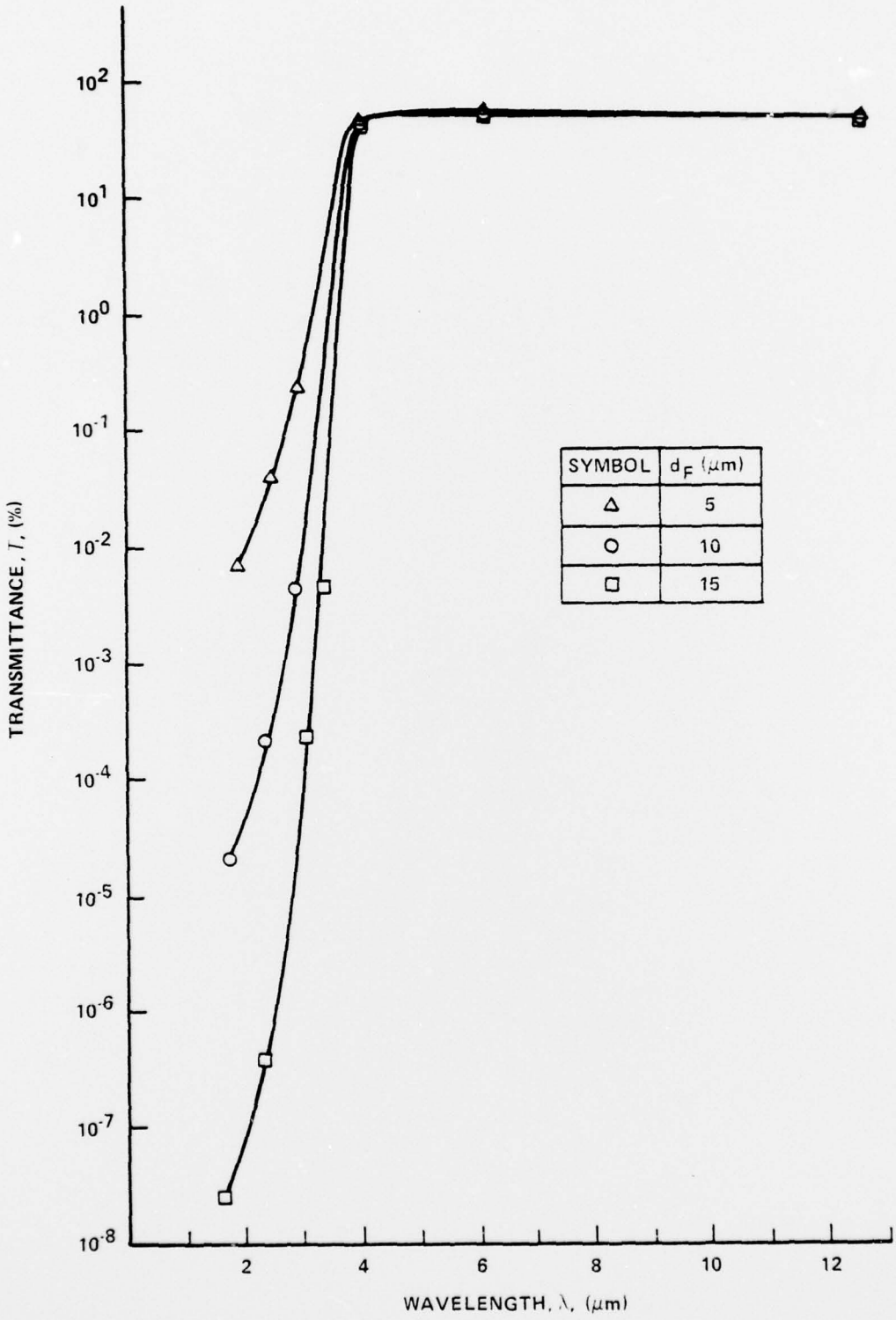

FIGURE 7. TRANSMITTANCE, T, FOR VARIOUS PbS FILTER THICKNESSES, d_F

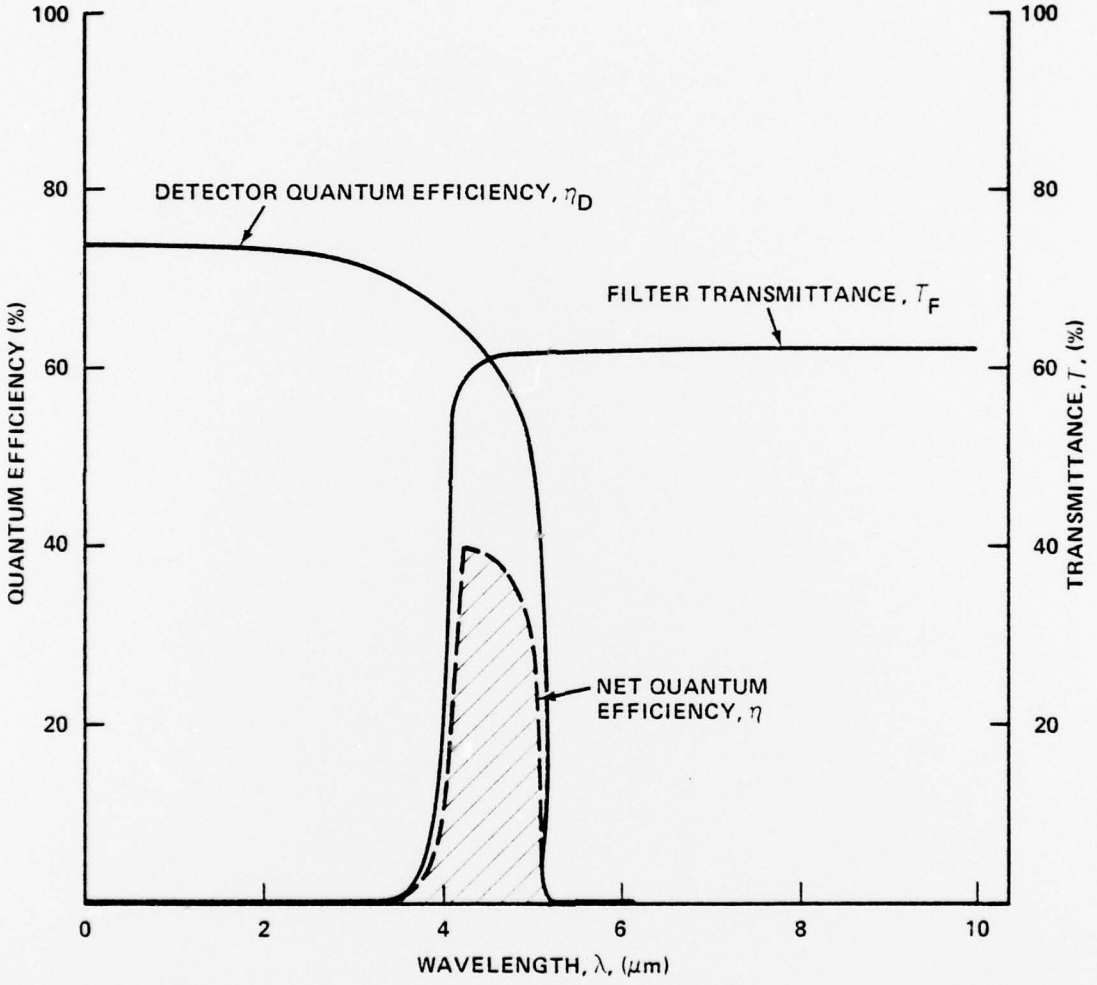

FIGURE 8. NET QUANTUM EFFICIENCY, η, OF SFD DEVICE

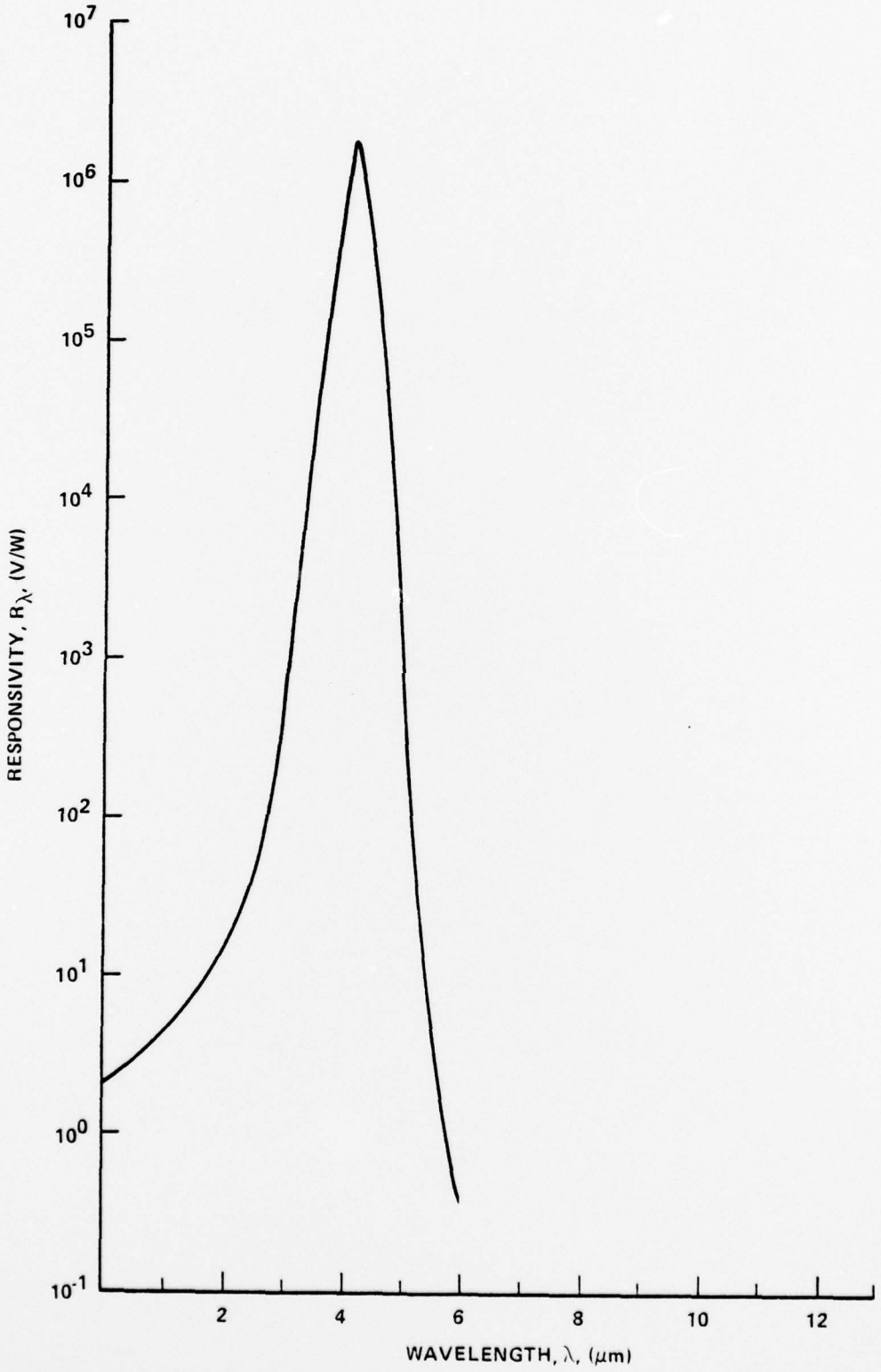

FIGURE 9. PREDICTED SPECTRAL RESPONSIVITY, R_λ, OF SFD DEVICE

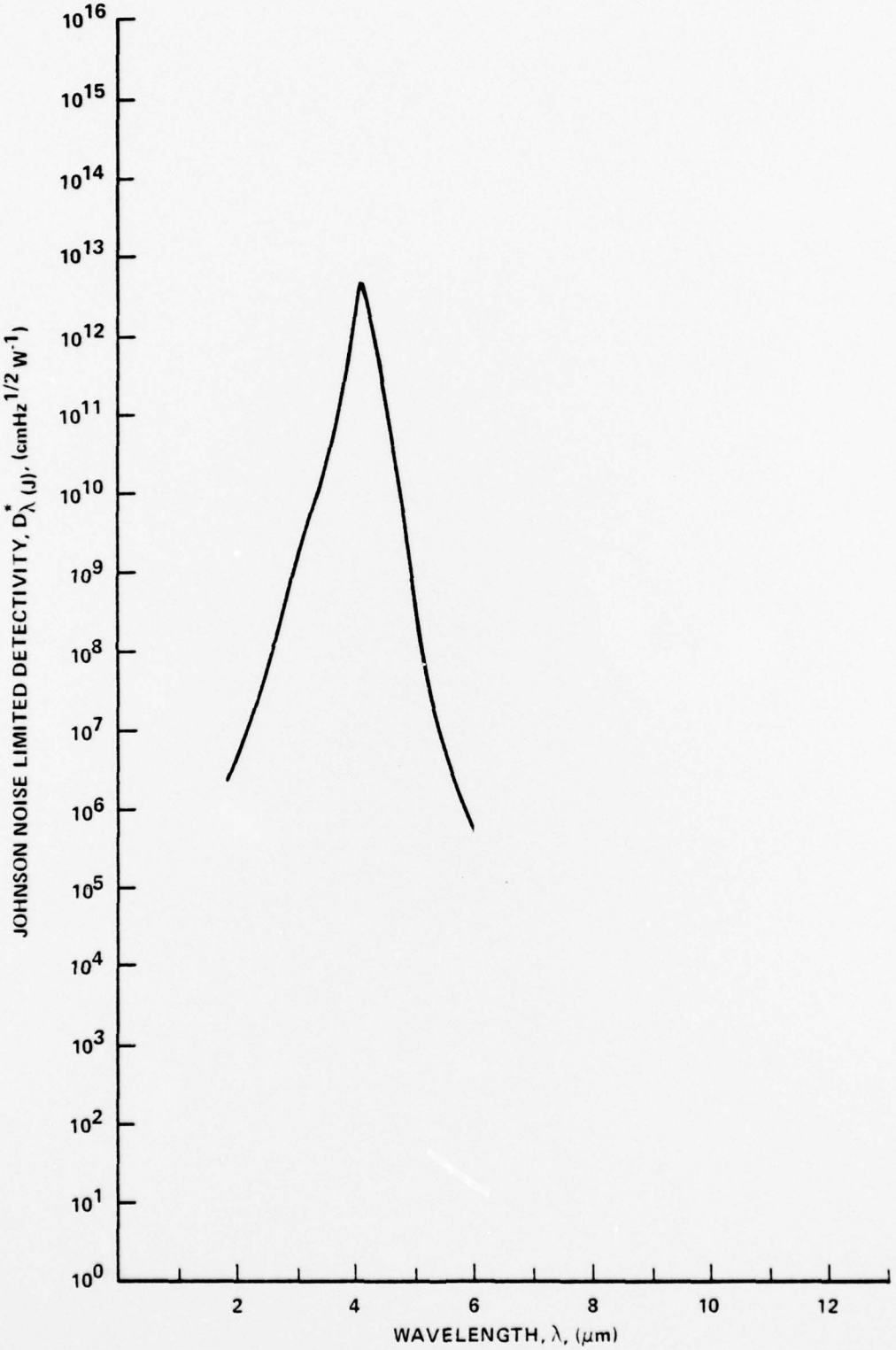

FIGURE 10. PREDICTED JOHNSON NOISE SPECTRAL DETECTIVITY, $D^*_{\lambda\,(J)}$, OF SFD DEVICE

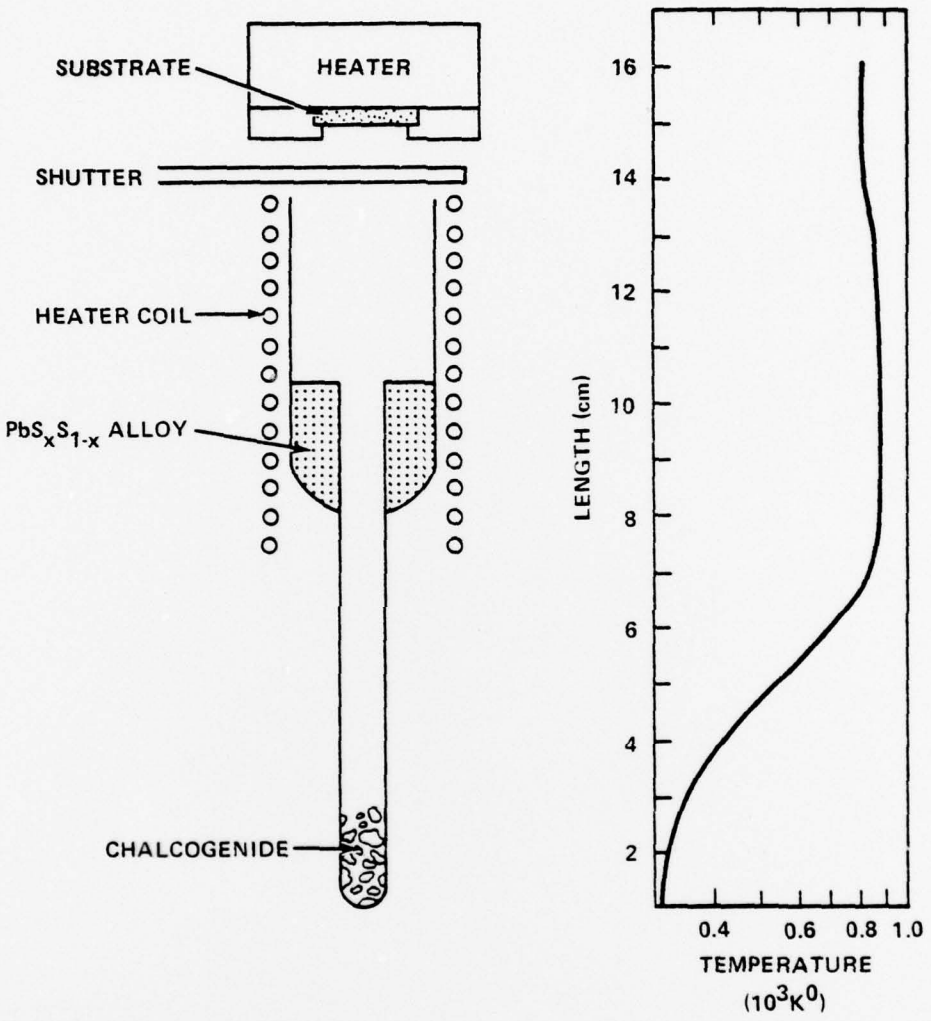

FIGURE 11. SCHEMATIC DIAGRAM OF APPARATUS USED TO GROW PbS_xSe_{1-x} EPITAXIAL FILMS WITH ASSOCIATED TEMPERATURE PROFILE.

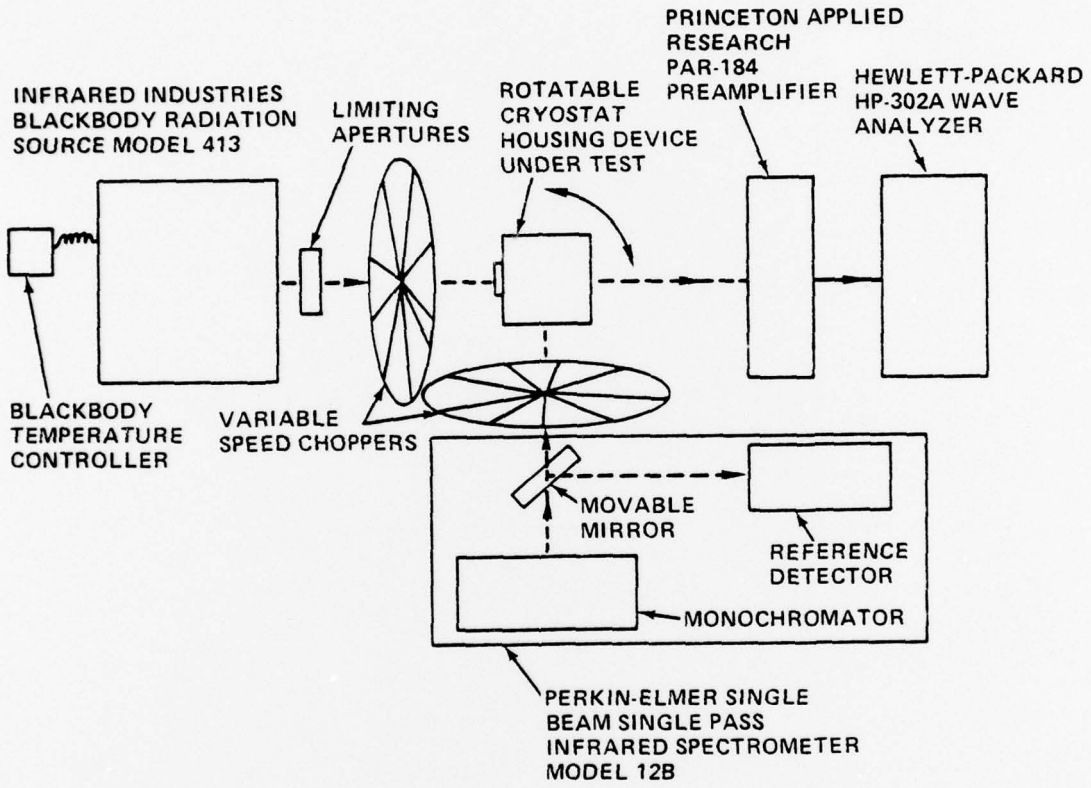

FIGURE 12. SCHEMATIC OF THE INFRARED DETECTOR TESTING SYSTEM.

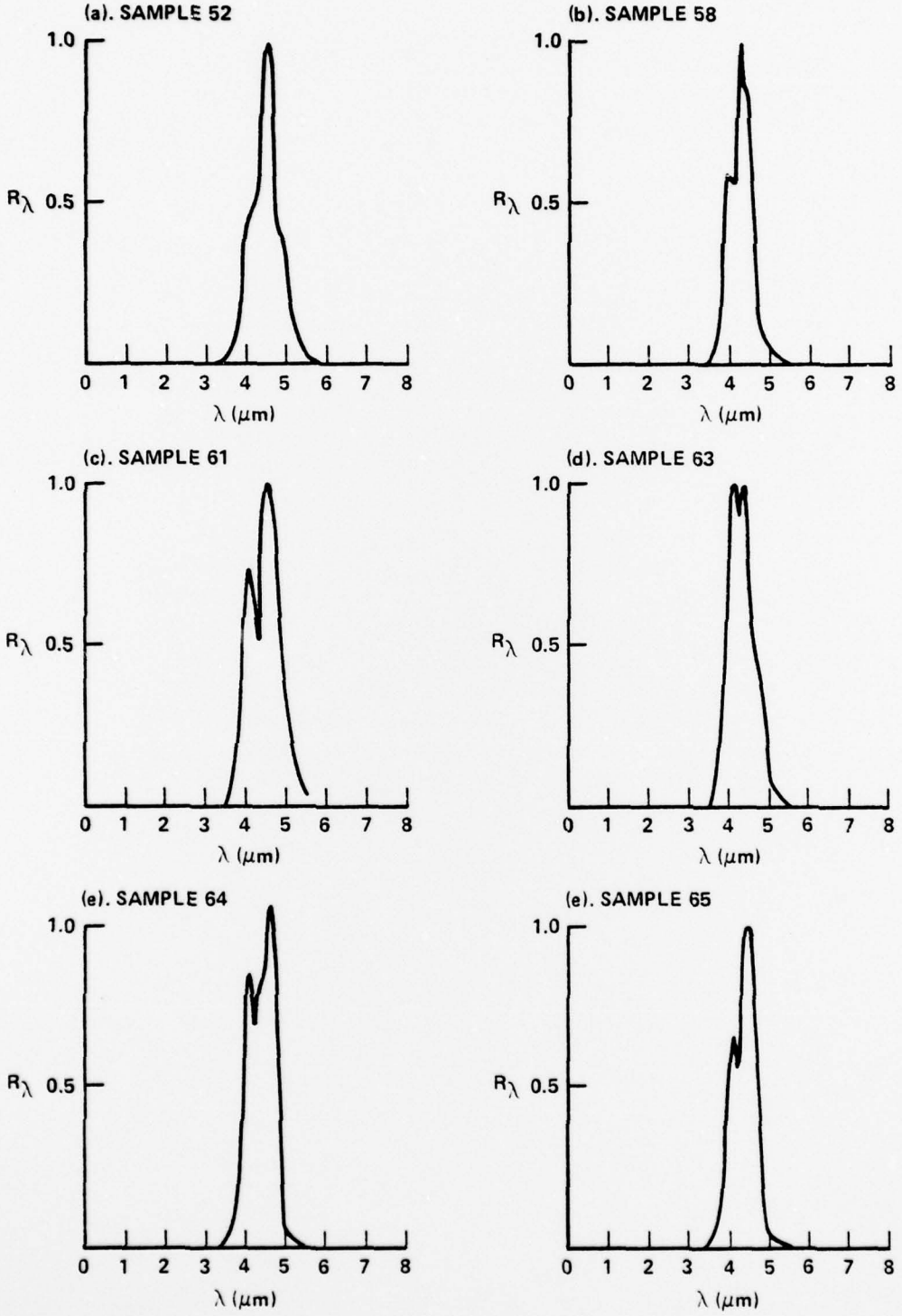

FIGURE 13. THE RELATIVE SPECTRAL RESPONSIVITY, R_λ (ARBITRARY UNITS), OF SIX SFD DEVICE SAMPLES AT 77°K.

LIST OF REFERENCES

1. Schoolar, R. B., Jensen, J. D. and Black, G. M., "Composition-tuned PbS_xSe_{1-x} Schottky-barrier infrared detectors," Applied Physics Letters, v. 31, no. 9, p. 620-622, 1 November 1977.

2. Sze, S. M., Physics of Semiconductor Devices, p. 11-146, Wiley, 1969.

3. Handbook of Military Infrared Technology, p. 58-70, 96-100, Office of Naval Research, Department of the Navy, Washington, D.C. 1965.

4. Bernig, P. H. and others, Physics of Thin Films, v. 1, p. 69-120, Academic Press, 1963.

5. Zemel, J. N., Jensen, J. D. and Schoolar, R. B., "Electrical and Optical Properties of Epitaxial Films of PbS, PbSe, PbTe, and SnTe," The Physical Review, v. 140, no. 1A, p. A330-A342, 4 October 1965.

6. Handbook of Chemistry and Physics, 41st ed., p. 2930, Chemical Rubber Publishing Company, 1959.

7. Prakash, V., "The Optical Absorption Edge in the Lead Salts and Its Variation With Temperature and Pressure," Ph.D. Thesis, Harvard University, 1967.

8. Scanlon, W. W., and others, Solid State Physics, J. 9, p. 83-137, Academic Press, 1959.

9. Dalven, R., "A Review of the Semiconductor Properties of PbTe, PbSe, PbS, and PbO," Infrared Physics, v. 9, p. 141-177, 1969.

10. Bouley, A. C. and Schoolar, R. B., Electrical Characteristics and Barrier Profiles of Photovoltaic Junctions of Lead Metal on Lead Sulphide Epitaxial Films, paper presented at the 20th Annual Electronic Materials Conference, Santa Barbara, California, 30 June 1978.

11. Schoolar, R. B., Jensen, J. D., Black, G. M. and Demske, D. L., Composition Tuned II-IV-VI Alloy Semiconductor Infrared Detectors," p. 1-6, paper printed at the Meeting of the IRIS Specialty Group on Infrared Detectors, Colorado Springs, CO, 22-23 March 1977.

12. Infrared Technology: generation, transmission and detection, p. 235-264, Wiley, 1962.

13. Hudson, R. D. Jr., Infrared System Engineering, p. 267, 270, 321, Wiley, 1969.

14. Naval Ordnance Laboratory UNCLASSIFIED Technical Report 71-223, Preparation and Properties of Epitaxial Lead Sulfide Infrared Detectors, by R. B. Schoolar, p. 1-21, UNCLASSIFIED, 15 October 1971.

15. Bouley, A. C., private communication.

16. Jensen, J. D., and Schoolar, R. B., "Surface charge transport in PbS_xSe_{1-x} and $Pb_{1-y}Sn_{1-y}Se$," Journal of Vacuum Science and Technology, v. 13, no. 4, July/August 1976.

INITIAL DISTRIBUTION LIST

		No. Copies
1.	Defense Documentation Center Cameron Station Alexandria, Virginia 22314	2
2.	Library, Code 0142 Naval Postgraduate School Monterey, California 93940	2
3.	Department Chairman, Code 69 Department of Mechanical Engineering Naval Postgraduate School Monterey, California 93940	1
4.	Professor A. E. Fuhs, Code 69Fu Department of Mechanical Engineering Naval Postgraduate School Monterey, California 93940	2
5.	Mr. R. B. Schoolar, Code R45 Naval Surface Weapons Center White Oak, Silver Spring, MD 20910	2
6.	LCDR R. A. Fantauzzo, USN RR #1 Amity Lake Road Belmont, NY 14813	2
7.	Librarian Naval Surface Weapons Center Dahlgren, Virginia 22448	1
8.	Librarian Naval Surface Weapons Center White Oak, Silver Spring, MD 20910	1
9.	Commander Destroyer Squadron Twelve FPO New York, New YOrk 09501	1
10.	Code R45 Naval Surface Weapons Center White Oak, Silver Spring, MD 20910	2
11.	Library U.S. Naval Academy Annapolis, MD 21412	1

12. Director 1
Air Force Weapons Laboratory
Kirtland AFB, NM 87117

13. COL. J. C. Rich USAF 1
Head
Advanced Radiation Technology Office F/AR
Kirtland AFB, NM 87117

14. Dr. Tien F. Tao 1
Naval Postgraduate School
Monterey, California 93940